Journal of Molecular and Cellular Cardiology 217 (2026) 176–188

Contents lists available at ScienceDirect

Journal of Molecular and Cellular Cardiology

journal homepage: www.elsevier.com/locate/yjmcc

Ca^{2+} current involvement in a KCNH2 mutation's phenotype and its modulation by estrogen

C. Maniezzi [a], F. Bastaroli [b], I. Anzaldi [a], C. Florindi [a], V. Dusi [c], A. Dosio [b], M. Mura [b], J. Tomek [d], J.F. Rodriguez Matas [e], F. Lodola [a], M. Gnecchi [b,f,*], A. Zaza [a,**]

[a] Department of Biotechnology and Biosciences, University of Milano-Bicocca, Milan, Italy
[b] Cardiothoracovascular Department, Translational Cardiology Unit, Fondazione IRCCS Policlinico San Matteo, Pavia, Italy
[c] Department of Medical Sciences, University of Turin, Turin, Italy
[d] Department of Anatomy, Physiology, and Genetics, University of Oxford, Oxford, United Kingdom
[e] Department of Chemistry, Materials and Chemical Engineering "Giulio Natta", Politecnico di Milano, Milan, Italy
[f] Department of Molecular Medicine, Unit of Cardiology, University of Pavia, Pavia, Italy

ARTICLE INFO

Keywords:
LQT2
KCNH2-G628S
I_{CaL}
Estradiol

ABSTRACT

Background: Estrogens affect repolarization and may act as phenotype modifiers in long QT syndrome (LQTS). In a LQT2 patient with the G628S-KCNH2 mutation (normal CACNA1C genes) the occurrence of arrhythmia-related symptoms followed 17-β estradiol (E2) administration. This study aims to test whether a mechanistic link can be established between the two events.

Methods: Membrane potential, I_{CaL} and I_{Kr} were measured from mutant (LQT2) and wild-type (WT) hiPS-CMs exposed to 10 nM E2. Adequacy of E2 effects in accounting for patient's electrical phenotype was tested by in silico simulations using a "population" approach. Molecular characterization was carried out by qPCR and immunocytochemistry.

Results: LQT2 hiPS-CMs were characterized by marked prolongation of action potential duration (APD) and susceptibility to early afterdepolarizations (EADs), thus recapitulating the LQT2 phenotype. In LQT2 hiPS-CMs, I_{Kr} was absent, the I_{CaL} window was increased and the recovery from inactivation was delayed. E2 reversed mutation's effects on APD and I_{CaL} window, but failed to restore I_{Kr} and reduce EADs prevalence. E2 also introduced a fast component in I_{CaL} recovery which contributed to I_{CaL} availability during the AP plateau. E2 did not change the expression of KCNH2 channels, E2 receptors (GPER) and CaV1.2 channels (CACNA1C). Simulations indicate that the changes in I_{CaL} gating are a major determinant of APD prolongation and EADs associated with the KCNH2 mutation.

Conclusions: The KCNH2 mutation was associated with I_{CaL} gating abnormalities crucially contributing to APD prolongation, which were largely corrected by E2. However, by accelerating I_{CaL} recovery, E2 facilitated EADs despite APD shortening.

1. Introduction

Genetic defects associated with delayed repolarization (Long QT Syndrome, LQTS) are characterized by highly variable penetrance and expressivity, their clinical phenotype ranging from nil to intractable arrhythmias among sibling carriers of the same mutation [1]. This observation suggests the involvement of "modifiers", genetic or not, either amplifying or blunting the primary effect of the mutation [2,3]. Such modifiers may modulate the arrhythmia substrate or, if powerful enough, act as arrhythmia triggers.

Repolarization is physiologically slower in females than in males, a difference reflected in the higher arrhythmogenic risk associated with pathogenetic or likelypathogenetic variant-induced repolarization abnormality after puberty [4]. This likely results from the opposite effect of estrogens and androgens on the expression and gating of channels contributing to repolarization reserve. Progesterone also plays a minor role in this scenario by shortening ventricular repolarization [5]. Thus, estrogens, or an unbalance between them and androgens, are likely

* Corresponding author at: Cardiothoracovascular Department, Translational Cardiology Unit, Fondazione IRCCS Policlinico San Matteo, Pavia, Italy.
** Corresponding author at: Department of Biotechnology and Biosciences, University of Milano-Bicocca, Milan, Italy.
E-mail address: antonio.zaza@unimib.it (A. Zaza).

https://doi.org/10.1016/j.yjmcc.2026.07.004
Received 25 February 2026; Received in revised form 3 July 2026; Accepted 6 July 2026
Available online 7 July 2026

candidates as enhancers of LQTS variants related phenotype. This view is supported by the case of a young female, carrier of an LQT2 related pathogenetic variant (KCNH2-G628S) under treatment with a monophasic combined estrogen-progestin oral pill for a policystic ovary syndrome (PCOS). The patient suffered a severe electrical storm shortly after resuming estrogen-progestin medication. By exploiting cardiomyocytes obtained from this patient, the present work tests whether estrogen (E2) challenge on the LQT2 substrate may affect repolarization and trigger arrhythmias, thus establishing a causal link of clinical relevance. Ventricular cardiomyocyte derived from patient's pluripotent stem cells (hiPS-CMs) were used as experimental model. E2 effect on a wild type (WT) genetic background were also tested.

The results obtained indicate that the G628S-KCNH2 mutation alters the CACNA1C channel gating, an action reversed by E2, which nonetheless failed to prevent EADs. Incorporation of such observations in a computational model supports the crucial role of I_{CaL} abnormalities in the LQT2 phenotype and explains the apparently paradoxical effect of E2. The observations disclose an unforeseen functional crosstalk between I_{Kr} and I_{CaL}; elucidation of its molecular mechanism awaits specifically designed studies, beyond the scope of the present work.

2. Methods

Essential information is given here; a detailed description of methods is provided in the Supplement.

2.1. Sample collection

The study and the protocols for sample collection were conducted in accordance with the Declaration of Helsinki and approved by the Ethic Committee of the Fondazione IRCCS Policlinico San Matteo. The goal of the study and the procedure for sample collection were explained to both the healthy donor and the patient in detail, and both subjects signed an informed consent for inclusion before they participated in the study.

2.2. Induced pluripotent stem cells and cardiomyocyte preparation

Induced pluripotent stem cells (hiPSs) from an LQT2 patient were generated by reprogramming dermal fibroblasts isolated from skin biopsy with the ReproRNA™-OKSGM kit (STEMCELL Technologies). hiPSs from healthy donor (WT genotype) were generated by reprogramming peripheral blood mononuclear cells (PBMCs) isolated from blood sampling, with the CytoTune™-iPS 2.0 Sendai Reprogramming Kit (ThermoFisher Scientific). Both hiPS lines were cultured in TeSR-E8 medium (STEMCELL Technologies) (37 °C and 5% CO2) and subsequently differentiated into hiPS-derived cardiomyocytes (hiPS-CMs) using the STEMdiff™ Ventricular Cardiomyocyte differentiation kit (STEMCELL Technologies™). The hiPS-CMs were maintained in RPMI 1640 Medium (Gibco®) with 1× B27 Supplement (Gibco®), 50 U/mL penicillin (Gibco®) and 50 U/mL streptomycin (Gibco®) before the experiments. More details can be found in the Supplementary material.

2.3. Electrophysiology

Electrophysiological experiments were carried out by whole-cell patch-clamp on hiPS-CMs at a slightly subphysiological temperature (30 °C) as required to improve preparation stability. As said, the cells obtained from the mutation carrier (LQT2 cells) were compared to those obtained from a healthy donor (WT cells). Before measurements, LQT2 and WT cells were incubated in 10 nM E2 for 10 min. This E2 concentration, while about tenfold the plasma levels present during an ovarian cycle (1–2 nM) [5], are at the threshold for hiPS-CMs modulation [6].

2.3.1. I-clamp

Spontaneous action potentials (APs) were recorded during the perfusion of standard external solution at 30 °C. The following parameters were measured: i) rate-corrected (Fridericia) action potential duration (c_APD) at 50% (c_APD_{50}) and 90% (c_APD_{90}) of repolarization, ii) triangulation index (c_APD_{90}/c_APD_{50}); iii) AP amplitude (mV), iv) AP rate (b/min), v) maximum diastolic potential (MDP, mV), vi) AP threshold potential (mV), vii) the gap between AP threshold and MDP (AP threshold – MDP, mV), viii) diastolic depolarization rate (DDR, V/s).

2.3.2. V-clamp

The quasi steady-state net membrane current (I_{net}) was recorded at 30 °C during a slow descending V ramp (−0.63 V/s) from +20 mV to −120 mV. Membrane slope conductance was calculated from I_{net} between −10 mV and −40 mV, encompassing the V range of early afterdepolarizations (EADs) occurrence.

The rapid delayed rectifier current (I_{Kr}) was recorded at 30° by a step protocol from a holding potential of −40 mV. I_{Kr} is small in hiPS-CMs [3], to resolve it accurately extracellular K^+ was increased to 5.4 mM and the current recorded after its blockade (by 2 μM E-4031) was digitally subtracted. I/V relationships were obtained for the current at the end of the activating step (I_{ss}) and for the tail current (I_{tail}). Maximal conductance was calculated from I_{tail} amplitude after activation at saturating potentials.

The L-type voltage-gated calcium current (I_{CaL}) was recorded at 27 ± 0.5 °C (to minimize run-down) with external and intracellular solutions minimizing contamination by other currents (see supplement). Maximum current density (I_{max}) and channel conductance (G_{max}) were estimated from peak I_{CaL} I/V relationships. I_{CaL} steady-state (ss) activation (d) and inactivation (f) curves were obtained with the appropriate protocols (see Supplement); mid activation/inactivation potentials ($V_{0.5}$) and slope factors were estimated by Boltzmann fitting of data points. The magnitude of I_{CaL} "window" was quantified as the area of overlap (d*f > 0) between the ss activation and inactivation curves. I_{CaL} activation/inactivation kinetics (τ_d and τ_f) were quantified by mono-exponential fitting. I_{CaL} Ca^{2+}-dependent inactivation (CDI) was estimated by comparing currents recorded within the same cell with Ba^{2+} (I_{BaL}) and Ca^{2+} (I_{CaL}) respectively as charge carriers; CDI was expressed as the difference between normalized I_{BaL} and I_{CaL} at 20 ms (r20) after current peak. The kinetics of I_{CaL} recovery from inactivation was assessed by a paired-pulse (p_1-p_2) protocol (steps to 0 mV from a holding V = −40 mV, close to the AP plateau of hiPS-CMs) with incremental p_1-p_2 intervals; recovery was quantified as the ratio of peak current amplitudes (Ip2/Ip1); the recovery time-constant (τ_{rec}) and Y intercept (offset) were estimated by mono-exponential fitting of the full recovery process.

All currents were normalized to membrane capacitance and expressed as current density (pA/pF).

2.4. Numerical simulations

With the aim of predicting how the changes experimentally observed in hiPS-CMs might impact on the electrical activity of mature cardiomyocytes, we implemented them in the O'Hara-Rudy model of the mature human action potential [7] (with minor modifications, detailed in the Supplement), taken to represent the WT genotype. The LQT2 model was generated from the WT one by modifying its parameters to reproduce, as closely as possible, the changes observed between WT and LQT2 hiPS-CMs for what concerns action potential duration, I_{CaL} gating properties and EADs prevalence. To keep into account the quantitative differences between hiPS-CMs and mature ones, we chose to reproduce experimentally observed changes as percentage variation from the WT value, rather than in absolute terms.

The model does not include a separate "recovery" transition for the voltage-dependent inactivation (f) gate [7], i.e. precisely the one slowed by the mutation and accelerated by E2. However, the kinetics of I_{CaL} recovery could be modulated, without perturbing inactivation kinetics, through changes in the time constant of the recovery from calcium

dependent inactivation gate for I_{CaL}, JCa (TauJCa, contained in the model I_{CaL} formulation and referred as τ_{rec} in this manuscript).

The LQT2 + E2 model was obtained from the LQT2 one by introducing the E2-induced changes in I_{CaL} gating observed in hiPS-CMs. Model output was analyzed after 5 min of stimulation at 1 Hz, adequate to achieve steady state.

To explore the effect of parameters variability in models' output (AP profile and EADs prevalence), a "model population" was obtained from each model (WT, LQT2 and LQT2 + E2) by a Montecarlo simulation [8]. Each model population contained 132 versions generated by introducing a ± 15% random variability in the model parameters (main ionic current conductances) [8] [9]. The range of c_APD values thus obtained for the WT model population did not exceed that of normal human QTc intervals; therefore, no further calibration was necessary.

The outputs of model populations were compared by statistical analysis. Model equations were integrated with an adaptive time step algorithm for stiff ordinary differential equations available in Matlab R2024 (Mathworks Inc).

2.5. Data analysis and statistics

Data analysis was performed off-line using Clampfit 10.7 software (Axon Instruments Inc., Burlingame, CA, USA). GraphPad Prism 8.0.2 (GraphPad software, San Diego California) was used for statistical analysis. Two-tailed unpaired Student's *t*-test was used to compare the means of independent samples; Fisher test with Benjamini-Hochberg post-hoc correction was used for categorical variables. Even if multiple comparisons were not required by study design, the difference among means of the same variable was preliminarily tested by ANOVA. In figures individual data points were plotted, to illustrate dispersion, along with the sample mean ± SEM. The number technical replicates (n) and the number of biological replicates (N) are reported in figure legends.

3. Results

3.1. Mutation carrier

A young female, with a positive family history for sudden death, had been under treatment for polycystic ovary syndrome (PCOS) for 3 years with a monophasic estro-progestinic preparation (EP), containing synthetic agonists of progesterone (desogestrel 150 μg) and estrogen (etinilestradiol 20 μg) receptors. Medication intake was irregular because of poor patient's adherence. At the age of 19 (under EP treatment), the patient suffered a likely arrhythmic, stress-related, syncopal episode, but didn't seek medical attention. At 21 years old she suffered a severe electrical storm with several self-limiting torsade the pointes (TdP) episodes, leading to syncope, and one case of TdP degeneration into ventricular fibrillation (VF) requiring DC-shock. Notably, the patient had just resumed the EP pill prematurely, i.e. before the planned monthly gap was completed. After stabilization, the ECG showed a markedly prolonged QTc (> 600 msec) and T wave abnormalities suggestive of a LQT2 genotype. A mild hypokalaemia was noticed (3.4 mEq/L), while magnesium was tested only after supplementation. After the initial treatment, the patient was subjected to left cardiac sympathetic denervation, supplemented by nadolol 1.2 mg/Kg/die, and a loop recorder was implanted. Under this regimen, the patient never suffered recurrences despite the persistence of a QTc > 500 msec. Estrogen administration was never resumed; after 2 uneventful years, a progestinic-only therapy for PCOS was started and was well tolerated. Of note, a sexual hormone panel performed in the acute phase showed relatively low testosterone level, which progressively raised during the follow up, as expected from EP discontinuation in PCOS.

Genetic screening detected in the patient the heterozygous KCNH2 variant G628S (c.1882G > A), a loss-of-function pore mutation with defective ion permeation but normal channel processing and trafficking (class 4) [10]; the other genes included in the screening panel, notably including those encoding for the Ca^{2+} channel main (CACNA1C) and accessory subunits, (CACNA2D1 and CACNB2) were normal.

3.2. Experimental results

3.2.1. hiPS-CMs molecular characterization and protein expression

The complete characterization of the hiPS lines can be found in the Supplementary material (Fig. S1).

Besides structural proteins, we determined the expression of the KCNH2 channel and the three main estrogen receptors (GPER, ERα, ERβ) by immunostaining (Fig. 1 and S2). The KCNH2 channel signal was equally expressed in both WT and LQT2 cells, with the expected localization at the plasma membrane level. The G-protein coupled estrogen receptor (GPER), which acts through rapid, non-genomic pathways, was localized at the plasma membrane in both WT and LQT2 cells. ER α and ERβ receptors, which mediate the genomic effect, were localized in the nuclear/perinuclear region.

It has been reported that E2 stimulation may modulate potassium channel expression [11], and that E2 effect may be concentration-dependent [12]. Accordingly, we measured KCNH2 expression by qPCR (Fig. 1A) in both WT and LQT2 cells at baseline and after 10 min of E2 stimulation at concentration of 1, 10 and 50 nM. No significant differences emerged in both WT and LQT2 cells whether they were stimulated or not (Fig. 1A). At protein level, KCNH2 levels and its subcellular localization were comparable between WT and LQT2 cells at both baseline and after exposure to 10 nM of E2 for 10 min, taken as a reference condition because it was the same one used for the electrophysiological experiments (Fig. 1C). Since E2 effects on ionic channels are mostly mediated by activation of the G-protein associated membrane receptor (GPER) [5,13], we determined its expression at baseline and after E2 stimulation (Fig. 1B). GPER was expressed at the same level in unstimulated WT and LQT2 cells. Under E2 stimulation, no effects were observed in the WT cells; in LQT2 cells, GPER expression was unchanged at 1 nM and 10 nM E2, while it was increased when exposed to 50 nM E2 (Fig. 1B). Semi-quantitative evaluation by immunostaining showed a trend to more pronounced GPER membrane localization after E2 stimulation in LQT2 cells as compared to WT ones (Fig. 1D).

3.2.2. KCNH2 mutation's effect on action potential parameters and I_{Kr}

Action potential parameters were compared across the experimental groups according to the scheme: LQT2 vs WT, WT + E2 vs WT, LQT2 + E2 vs LQT2 (Fig. 2).

As compared to WT cells, LQT2 ones were characterized mainly by a marked prolongation of c_APD at all repolarization levels (c_APD_{90} + 142%; $p < 0.05$), without changes in the triangulation index (Fig. 2A). The spontaneous beating rate was consequently reduced (−49%; $p < 0.05$; Fig. S3), which was also the result of an increase in the gap between maximum diastolic potential (MDP) and threshold one (+ 94%; $p < 0.05$; Fig. S3). The remaining AP parameters, including diastolic depolarization rate (DDR), were unchanged (Fig. S3). Whereas early afterdepolarizations (EADs) never occurred in WT cells, they were observed in 13% of LQT2 cells (Fig. 2A and C); possibly due to the small prevalence of the phenomenon, the increment did not achieve statistical significance.

In WT cells, I_{Kr} had a mid activation potential ($V_{0.5}$) at −23.1 ± 3.9 mV, displayed the typical"inwardly rectifying" profile of I_{ss} and had a maximal (I_{tail}) conductance (G_{max}) of 54.5 ± 8.9 pS/pF. In WT cells E2 did not significantly change $V_{0.5}$, the I_{SS} profile and G_{max}. In LQT2 cells I_{Kr} was consistently unmeasurable, thus confirming high mutation's penetrance, and was not recovered by E2 (Fig. S4).

3.2.3. E2 effect on action potential parameters in WT and LQT2 cells

In WT cells E2 had only minor effects (Fig. S5A). AP amplitude was slightly reduced (−11%, $p < 0.05$); a trend in c_APD_{90} shortening (−16%, NS) was associated with a reduction in the triangulation index

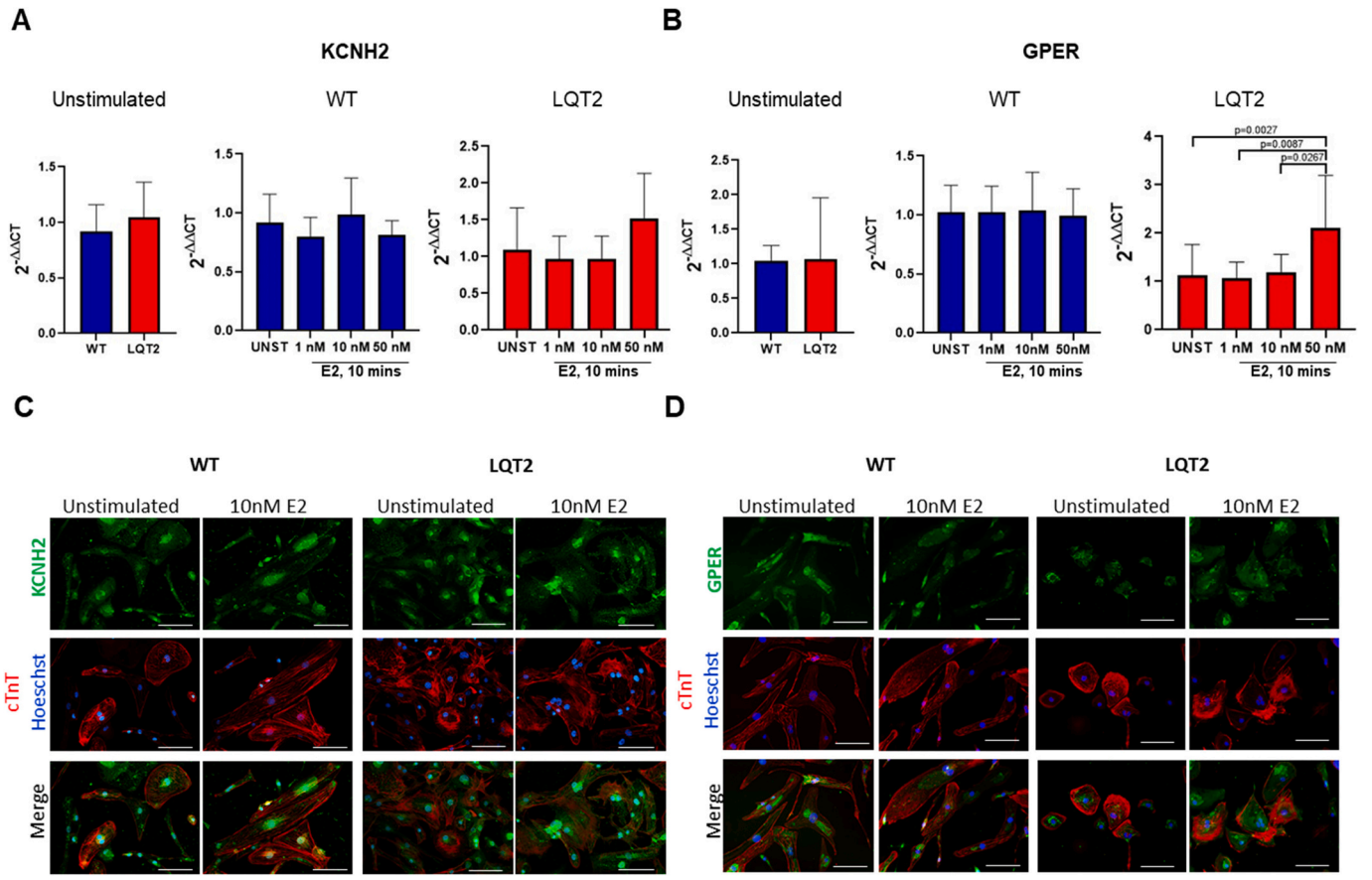

Fig. 1. KCNH2 and GPER expression before and after E2 stimulation. KCNH2 (A) and GPER (B) mRNA levels in WT (blue) and LQT2 (red) hiPS-CMs unstimulated, or stimulated for 10 min with 1, 10 or 50 nM of E2. The relative gene expression of both KCNH2 and GPER was quantified by qPCR using the $2^{-\Delta\Delta Ct}$ method, in RNA samples from $N = 3$ differentiations of WT and LQT2 hiPS-CMs. cTnT was used as reference gene for normalization. The bar graphs show the mean relative expression +/− standard deviation (unpaired *t*-test).

The mean of the unstimulated samples was used as a calibrator to calculate the ΔΔCt of the E2-stimulated samples. The data were analyzed using a one-way ANOVA test. * $p < 0.05$, ** $p < 0.01$. (KCNH2 $N = 3$ biological replicates; UNST WT: $n = 31$ technical replicates; WT 1 nM: $n = 12$ technical replicates; WT 10 nM: $n = 15$ technical replicates; WT 50 nM: n = 12 technical replicates; UNST LQT2: $n = 20$ technical replicates; LQT2 1 nM: $n = 9$ technical replicates; LQT2 10 nM: n = 9 technical replicates; LQT2 50 nM: n = 9 technical replicates; GPER N = 3 biological replicates UNST WT: $n = 22$ technical replicates; WT 1 nM: n = 12 technical replicates; WT 10 nM: n = 12 technical replicates; WT 50 nM: n = 12 technical replicates; UNST LQT2: n = 22 technical replicates; LQT2 1 nM: n = 9 technical replicates; LQT2 10 nM: n = 9 technical replicates; LQT2 50 nM: n = 9 technical replicates).

KCNH2 (C) and GPER (D) protein levels assessed by immunofluorescence in WT and LQT2 hiPS-CM, before and after 10 nM E2 stimulation for 10 min. KCNH2 and GPER proteins are in green, cardiac troponin cTnT is in red, nuclei counterstained with Hoechst 33258 in blue. Size bars: 100 μm. (For interpretation of the references to colour in this figure legend, the reader is referred to the web version of this article.)

(−24%, $p < 0.05$, i.e. c_APD_{50} shortened less than c_APD_{90}). E2 failed to affect the spontaneous beating rate and the parameters determining it, namely the gap between MDP and activation threshold and DDR; nonetheless, as absolute values, MDP and activation threshold were both slightly depolarized (Fig. S5A).

In LQT2 cells, E2 did not affect AP amplitude (Fig. S5B), but shortened c_APD_{90} significantly (−18%; $p < 0.05$) without affecting the triangulation index (i.e. c_APD_{90} and c_APD_{50} were similarly shortened, Fig. 2B). In a subset of cells E2 increased the spontaneous beating rate (+29%; $p < 0.05$; Fig. S5B), which was accounted for by a reduction of the gap between MDP and the activation threshold (−33%; $p < 0.05$; Fig. S3B); nonetheless, as population means, MDP and activation threshold were unaffected by E2 (Fig. S5B).

After exposure to E2, EADs occurred in 5% of WT cells and in 23% of LQT2 cells; only in the latter repetitive EADs were occasionally observed (Fig. 2B). Despite the clear-cut trend to increase in LQT2 cells exposed to E2 (Fig. 2C), EADs remained a rare phenomenon and the differences in their prevalence failed to achieve statistical significance (Fisher $p = 0.054$; corrected post-hoc $p = 0.076$).

The amplitude of phase 1 repolarization (hence the plateau potential) might theoretically affect the genesis of EADs; we tested for this possibility by measuring the c_APD_{30}/c_APD_{90} ratio, which reflects the extent to which phase 1 contributes to overall APD. The ratio was significantly smaller in LQT2 cells as compared to WT ones (Fig. S6A), as expected from predominant prolongation of phases 2 and 3 in LQT2, but it was unaffected by E2 (Fig. S6B). Furthermore, the ratio did not differ between cells with and without EADs (Fig. S6C). This rules out phase 1 amplitude as the determinant of EADs distribution across the experimental groups.

To summarize, in LQT2 cells only (genotype specific effect) E2 shortened c_APD and, if anything, tended to facilitate EADs. Both these findings were opposite to expectations; indeed, a) estrogens reportedly prolong APD and b) EADs are typically facilitated by APD prolongation (suppressed by APD shortening) [14]. Acute E2 exposure is known to reduce I_{Kr} [5], which would prolong c_APD instead; this and the complete lack of I_{Kr} in LQT2 cells (Fig. S4) led us to hypothesize the involvement of another current in modulation of the LQT2 phenotype by E2.

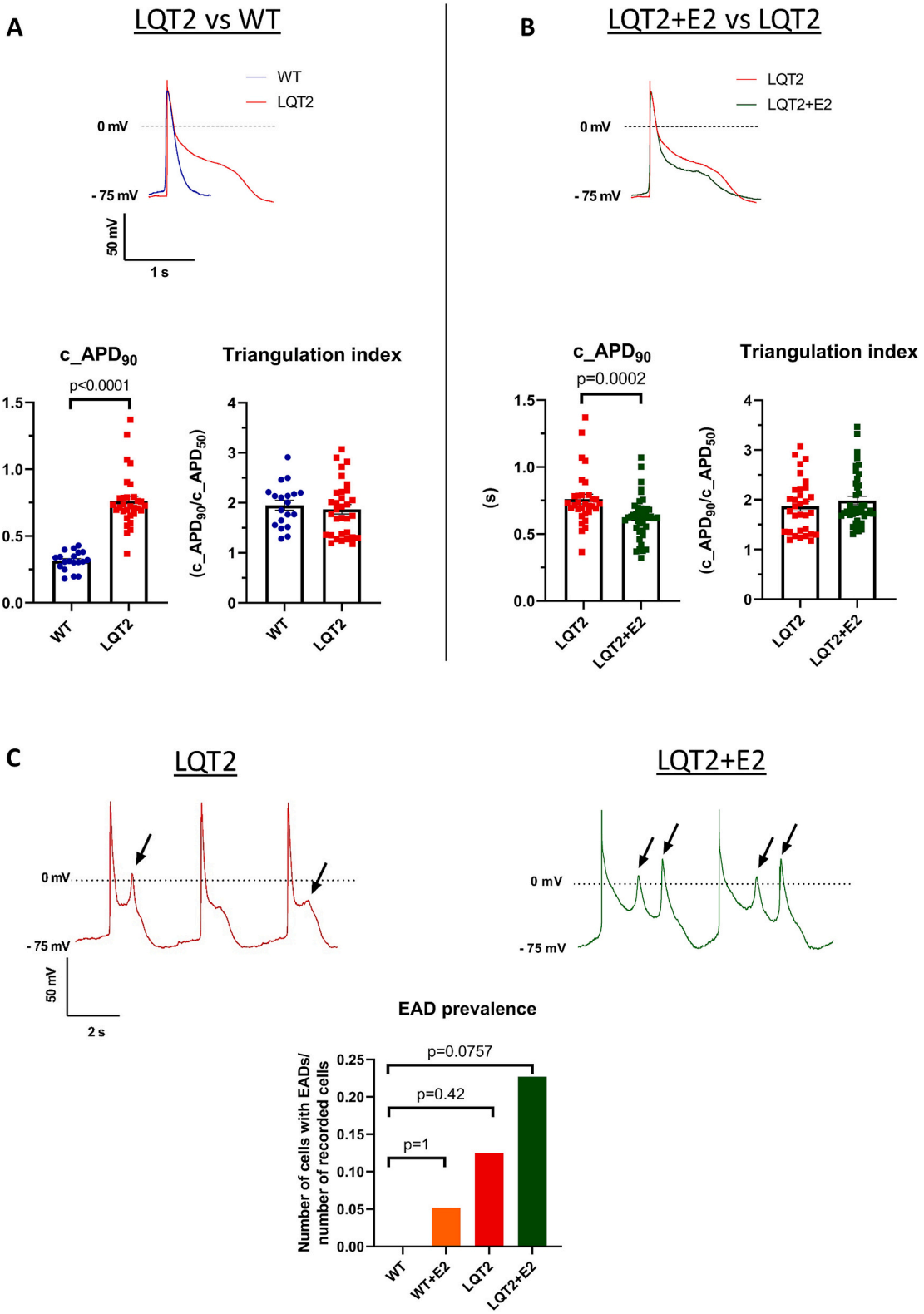

Fig. 2. Comparison between LQT2 and WT cells for AP parameters and their response to E2. Comparison LQT2 vs WT (A) and LQT2 + E2 vs LQT2 (B). (*Top*) Representative traces of AP recorded during spontaneous activity. (*Bottom*) Quantification of AP parameters (WT: $n = 19$ technical replicates, N = 3 biological replicates; LQT2: $n = 32$ technical replicates, $N = 4$ biological replicates; LQT2 + E2: $n = 44$ technical replicates, N = 4 biological replicates). (C) (*Top*) Representative EADs (arrows) in LQT2 and LQT2 + E2. (*Bottom*) EAD prevalence. (WT: n = 19 technical replicates, N = 3 biological replicates; LQT2: n = 32 technical replicates, N = 4 biological replicates; LQT2 + E2: n = 44 technical replicates, N = 4 biological replicates). *Unpaired t-test. Fisher test with Benjamini-Hochberg post-hoc correction.*

3.2.4. KCNH2 mutation's effect on quasi-steady-state (ss) net membrane current (I_{net}) and its response to E2

To obtain preliminary clues on the nature of the E2-sensitive conductance accounting for c_APD shortening, we compared the quasi-steady-state (ss) I/V curves of total membrane current (I_{net}) among the experimental groups. As shown in Fig. S7, roughly between −40 and −10 mV the I/V curves are characterized by a negative slope region, producing an inward notch. The depth of the notch was larger in LQT2 than in WT cells and returned toward the WT levels in LQT2 cells exposed to E2. Albeit I_{net} does not identify a specific current, the range of potentials encompassing the notch corresponded to the I_{CaL} "window" [14], as also reported in hiPS-CMs [15]. This suggested that the persistent (ss) component of I_{CaL} was enhanced in LQT2 cells, and a possible target of E2 modulation; therefore, we focused on detailed I_{CaL} evaluation.

3.2.5. KCNH2 mutation's effect on CACNA1C expression and I_{CaL} properties

3.2.5.1. CACNA1C expression. CACNA1C was expressed at same level in WT cells and LQT2 ones (Fig. S8).

3.2.5.2. I_{CaL} properties. Albeit mutation of a K^+ channel should not affect the Ca^{2+} current in principle, genotype-specificity of E2 effects on repolarization and I_{net} implied that I_{CaL} might differ between LQT2 and WT cells, which were therefore compared for this current. Maximum I_{CaL} density (I_{max}) and conductance (G_{max}) were similar between WT and LQT2 cells (Fig. 3A), suggesting unchanged membrane expression of the channel. Nonetheless, the steady-state "activation curve" of LQT2 cells was negatively shifted ($V_{0.5}$ –11 mV; $p < 0.05$, Fig. 3A) with respect to that of WT cells; since the "inactivation curve" was unchanged, this led to a substantial enhancement of I_{CaL} "window" (+83%; $p < 0.05$; Fig. 3A) in LQT2 cells. Notably, the "window" represents the range of membrane potentials at which I_{CaL} conductance differs from 0 even at steady-state, thus affecting repolarization.

The kinetics (time constants) of activation and inactivation failed to differ significantly between LQT2 and WT cells at all membrane potentials (Fig. 4A). I_{CaL} recovery from inactivation was instead remarkably (55%) slower in LQT2 cells than in WT ones ($p < 0.05$, Fig. 4A top), but it only marginally affected I_{CaL} availability at p_1/p_2 intervals in the hundred milliseconds range, i.e. those relevant to action potential repolarization (Fig. 4A bottom).

Ca^{2+} − dependent I_{CaL} inactivation (CDI) was unchanged between WT and LQT2 cells (Fig. 5A).

3.2.6. E2 effects on CACNA1C expression and I_{CaL} properties

3.2.6.1. CACNA1C expression. Exposure to 1, 10 or 50 nM E2 for 10 min did not alter the CACNA1C expression levels in WT cells (Fig. S8A). In LQT2 cells we observed a tendency to increase the CACNA1C expression at all concentrations tested, which however did not reach statistical significance (Fig. S8A). CACNA1C immunostaining (Fig. S8B) showed similar results: upon E2 stimulation there were no differences in the WT cells vs baseline, while a slight increase was present in LQT2 cells. Taken together, these results support the notion that exposure to the tested levels of E2 does not result in a biologically significant change in CACNA1C in either WT cells or LQT2 ones.

3.2.6.2. I_{CaL} properties. We then proceeded to test if I_{CaL} was modulated by E2 in WT and LQT2 cells respectively.

In WT cells, I_{CaL} gating parameters were globally insensitive to E2 (Fig. S9) and E2 failed to affect maximum I_{CaL} density and conductance (G_{max}) in both genotypes (Figs. 3B and S9). In LQT2 cells only, E2 positively shifted the steady state "activation curve" (V_{05} + 8 mV; $p < 0.05$, Fig. 3B), thus minimizing the difference in the I_{CaL} "window" between the two genotypes. E2 failed to affect activation and inactivation time constants significantly (Fig. 4B). On the other hand, changes in I_{CaL} recovery kinetics might theoretically explain the apparent conflict between E2 effect on c_APD and EADs of LQT2 cells (see discussion); therefore, we proceeded to its evaluation. E2 accelerated I_{CaL} recovery from inactivation (τ_{rec} − 26%; $p < 0.05$, Fig. 4B) again reversing the slowing associated with the KCNH2 mutation (compare with Fig. 4A). Notably, this also involved an increase in the recovery intercept (curve offset), i.e. the I_{CaL} density available at very short p_1-p_2 intervals, by 169% ($p < 0.05$; Fig. 4B). Overall, E2 more than doubled the I_{CaL} available in at p_1-p_2 intervals relevant to action potential repolarization in LQT2 cells (Fig. 4B). In WT cells I_{CaL} recovery rate was instead unchanged by E2 (Fig. S9), consistent with their overall insensitivity to the hormone.

Neither in WT, nor in LQT2 cells, E2 changed Ca^{2+} − dependent I_{CaL} inactivation (CDI) significantly (Fig. 5B and C).

3.3. Numerical simulations

Whereas the experiments were necessarily carried out in hiPS-CMs (immature cells), their results are of translational relevance if applied to mature human electrophysiology. This prompted us to implement the observed I_{CaL} changes in a computational model of adult human action potential in which the KCNH2 mutation was simulated. To incorporate variability and analyse the output statistically, we adopted the "model population" approach (see methods); therefore, modelling results are reported as population mean ± SE and $p < 0.05$ denotes significance of differences. In consideration of the differences between the electrophysiology of hiPS-CMs vs mature CMs, the model was parametrized to achieve the desired APD contours and EADs prevalence. To this end, all experimentally observed I_{CaL} changes were included in qualitative terms but, in the sake of model stability, their magnitude had to be somewhat limited (as detailed below).

3.3.1. Comparison between LQT2 vs WT model populations

To simulate the LQT2 phenotype, I_{Kr} conductance was reduced by 60%, of the original value. This prolonged APD from 314 ± 17 to 459 ± 16 ms (+46%; $p < 0.05$), a difference grossly underestimating the patient's QTc prolongation and the c_APD prolongation in LQT2 hiPS-CMs (+146%); notably, reducing I_{Kr} further only slightly affected APD (e.g. 70% block of I_{Kr} prolonged APD to 497 ms).

Including I_{CaL} changes (activation $V_{0.5}$ –7 mV and τ_{rec} + 20%), further prolonged LQT2 APD to 501 ± 25 ms ($p < 0.05$; +60%), thus approaching the experimental LQT2 values, and increased EADs prevalence to 8.0% (Fig. 6C). Under this condition, further I_{Kr} reduction was associated with an EADs prevalence well above the one experimentally observed, which approached 100% at 70% I_{Kr} reduction (Fig. 7A).

The mean contours of AP (excluding those with EADs) for WT (blue trace) and LQT2 (red trace) are shown in Fig. 6A.

Modelled I_{CaL} gating changes are illustrated in Fig. S10.

3.3.2. E2 effect on the LQT2 population

As dictated by the experimental observations, E2 effect on the LQT2 model was simulated by partial reversal of all mutation's effects on I_{CaL}, as experimentally observed. Shifting activation $V_{0.5}$ by +5 mV removed the late plateau phase, thus reducing APD to 467 ± 17 ms ($p < 0.05$); however, it completely suppressed EADs (results not shown). Including the acceleration of I_{CaL} recovery from inactivation (τ_{rec} − 35%) further reduced APD (mean APD profile in Fig. 6A as green line), but it increased EADs prevalence to 17% (Fig. 6B and C), thus reproducing the experimental observation of EADs facilitation despite APD shortening.

3.3.3. Sensitivity analysis

The model population strategy allowed to estimate the sensitivity of EADs prevalence to the ionic current changes caused by the mutation. The surface plot of Fig. 7A shows the EADs prevalence as a function of I_{Kr}

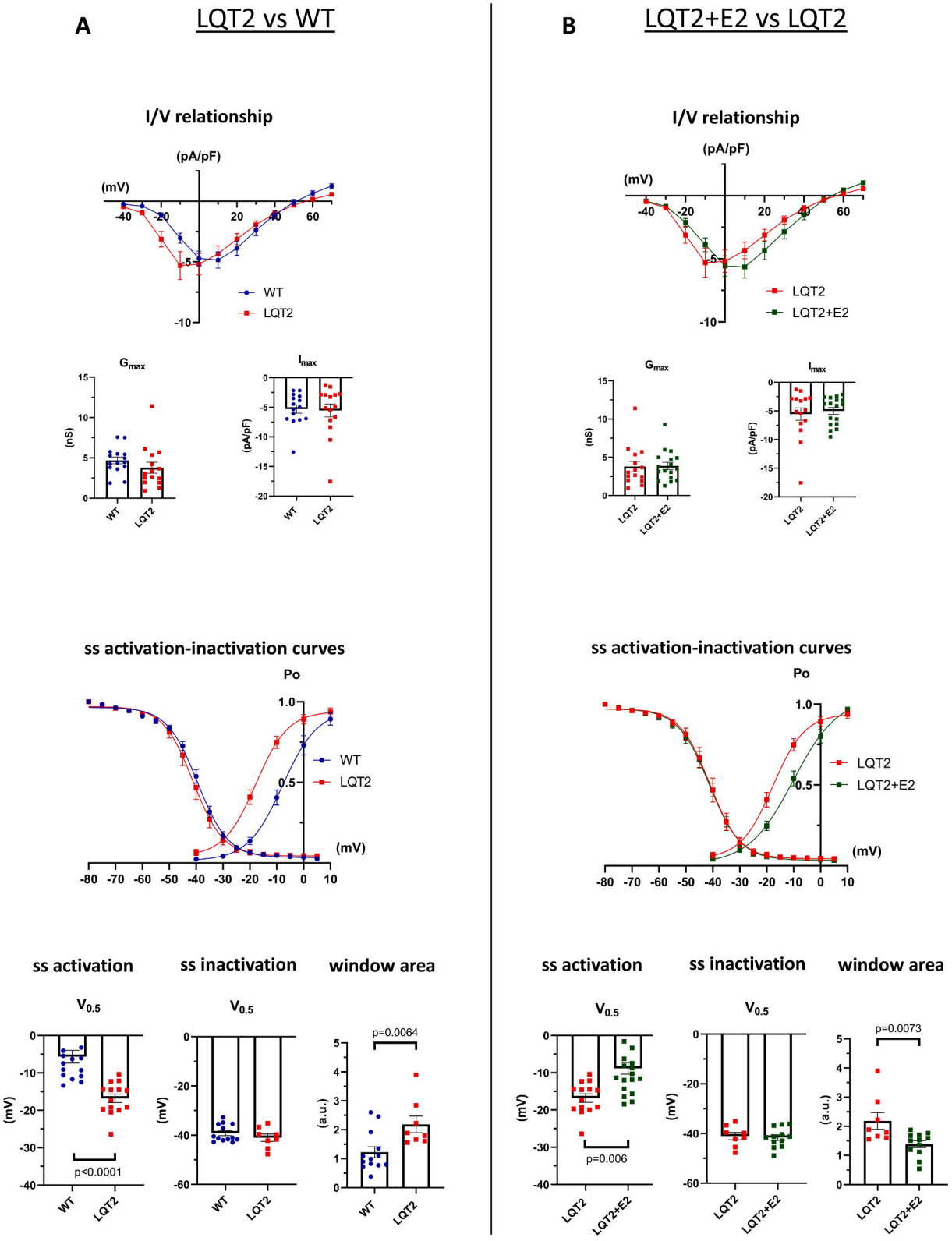

Fig. 3. Comparison between LQT2 and WT cells for I_{CaL} properties and their response to E2. Comparisons LQT2 vs WT (A) and LQT2 + E2 vs LQT2 (B). (*Top*) Peak I/V relationship with statistics for G_{max} and I_{max} (WT: $n = 15$ technical replicates, $N = 2$ biological replicates; LQT2: n = 15 technical replicates, $N = 2$ biological replicates; LQT2 + E2: $n = 17$ technical replicates, $N = 2$ biological replicates). (*Bottom*) Steady-state activation and inactivation curves with statistics for mid activation (WT: $n = 13$ technical replicates, N = 2 biological replicates; LQT2: $n = 14$ technical replicates, N = 2 biological replicates; LQT2 + E2: n = 19 technical replicates, N = 2 biological replicates) and inactivation potentials ($V_{0.5}$) (WT: n = 13 technical replicates, N = 2 biological replicates; LQT2: $n = 8$ technical replicates, $N = 2$ biological replicates; LQT2 + E2: $n = 12$ technical replicates, $N = 2$ biological replicates) and I_{CaL} window area (WT: $n = 13$ technical replicates, $N = 2$ biological replicates; LQT2: n = 8 technical replicates, N = 2 biological replicates; LQT2 + E2: n = 12 technical replicates, N = 2 biological replicates). *Unpaired t-test.*

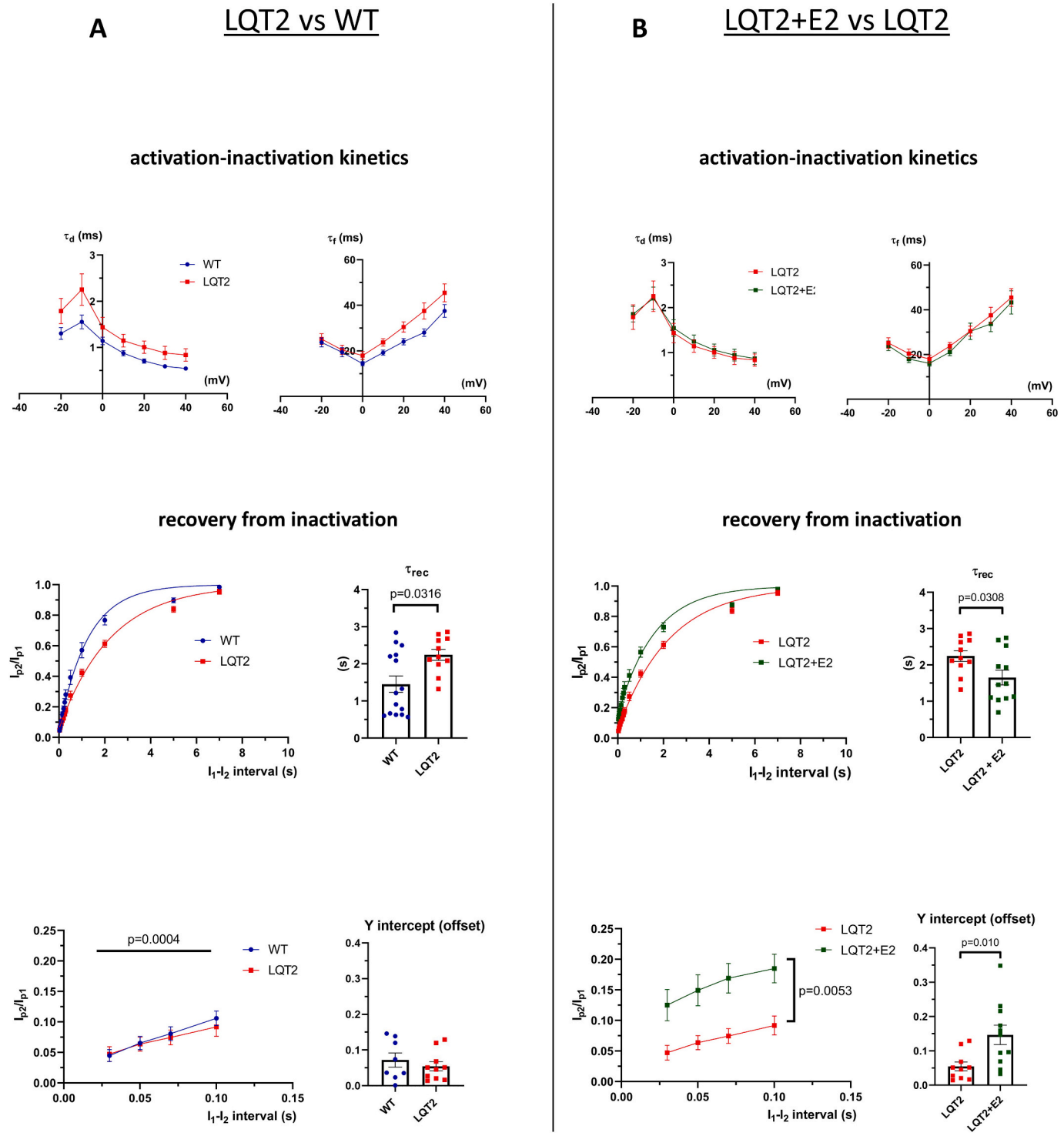

Fig. 4. Comparison between LQT2 and WT cells for I_{CaL} gating kinetics and its response to E2. Comparison LQT2 vs WT (A) and LQT2 + E2 vs LQT2 (B). (*Top*) Activation and inactivation time constant as a function of membrane potential (WT: $n = 15$ technical replicates, N = 2 biological replicates; LQT2: n = 15 technical replicates, N = 2 biological replicates; LQT2 + E2: n = 17 technical replicates, N = 2 biological replicates). (*Bottom*) Recovery from inactivation: full recovery curves and τ_{rec} statistics (WT: n = 15 technical replicates, N = 2 biological replicates; LQT2: $n = 11$ technical replicates, N = 2 biological replicates; LQT2 + E2: n = 12 technical replicates, N = 2 biological replicates); zoom on early recovery intervals (0–100 ms) and statistics for the Y intercept are shown below (WT: n = 8 technical replicates, N = 2 biological replicates; LQT2: $n = 10$ technical replicates, N = 2 biological replicates; LQT2 + E2: n = 11 technical replicates, N = 2 biological replicates). *Unpaired t-test. Two-Way ANOVA.*

reduction and I_{CaL} activation shift (δd_∞). Notably, up to 70% reduction in I_{Kr} fails to induce EADs unless I_{CaL} activation is also negatively shifted, with a threshold at about −5 mV. Above such threshold, EADs prevalence increases exponentially. Sensitivity of APD_{90} to the same parameters, shown in Fig. S11, is more linear that that of EADs, implying that over the critical range of parameters, the increase in EADs prevalence may not be proportional to APD prolongation.

The surface plot of Fig. 7B shows the EADs prevalence as a function

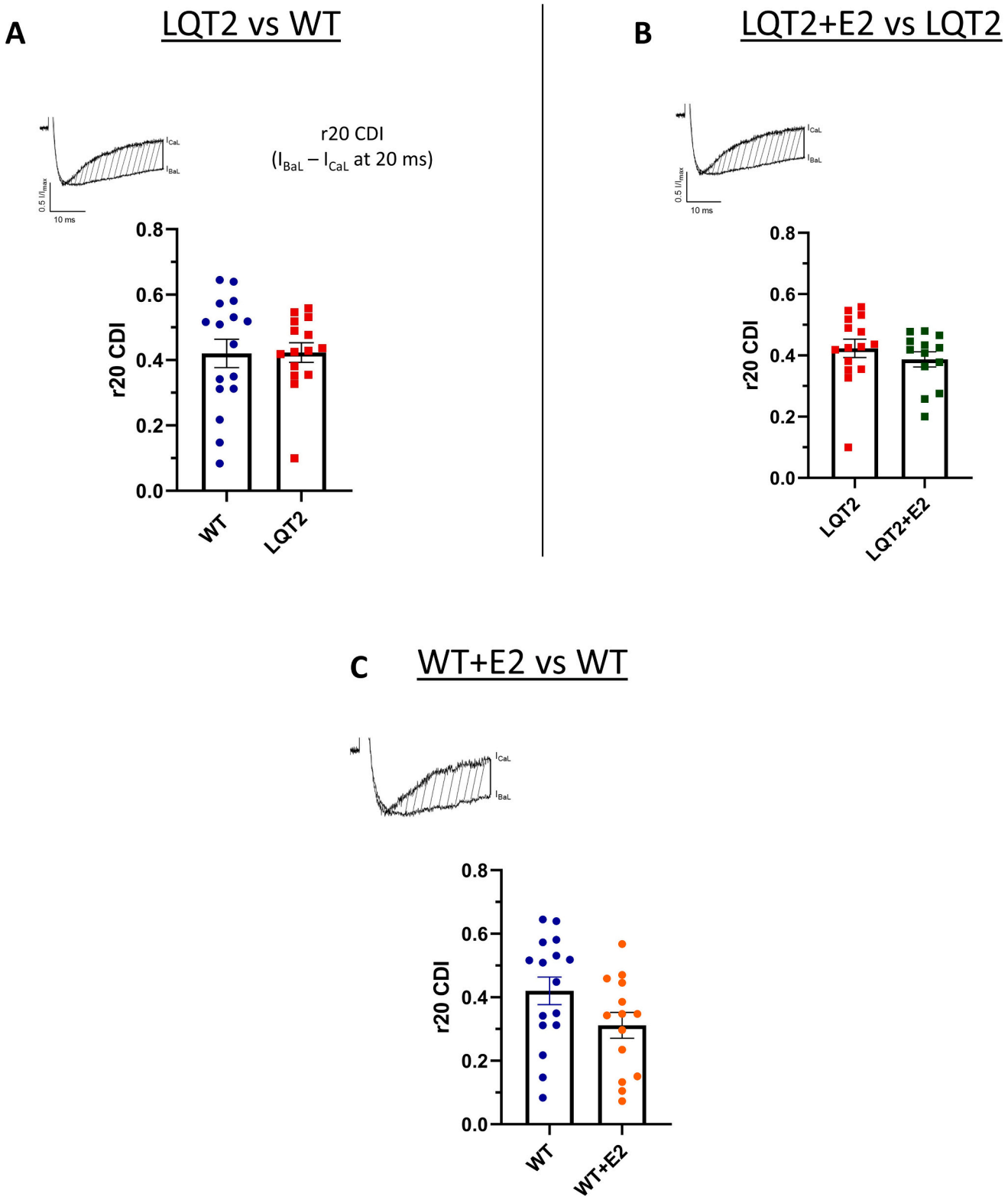

Fig. 5. Comparison between LQT2 and WT cells for Ca^{2+}-dependent inactivation (CDI) of I_{CaL} and its response to E2. Comparison LQT2 vs WT (A), LQT2 + E2 vs LQT2 (B) and WT + E2 vs WT (C). CDI denoted by the hatched area in the representative tracings of each panel and quantitated as difference between normalized I_{BaL} and I_{CaL} at 20 ms (r20) after current peak (WT: n = 16 technical replicates, N = 2 biological replicates; WT + E2: n = 14 technical replicates, N = 2 biological replicates; LQT2: n = 15 technical replicates, N = 2 biological replicates; LQT2 + E2: n = 13 technical replicates, N = 2 biological replicates). *Unpaired t-test.*

of I_{CaL} activation shift (δd_∞) and acceleration of recovery (τ_{rec} % reduction) at fixed (60%) I_{Kr} block. Acceleration of I_{CaL} recovery dramatically amplifies the effect of activation shifts on EADs prevalence. Notably, albeit achieving a 100% EADs prevalence, the parameters range explored slightly underestimates the changes observed in hiPS-CM (see above). By showing the "EADs isolines", Fig. 7C illustrates the relationship between δd_∞ shift and τ_{rec} % reduction at the same EADs prevalence (denoted by the small numbers on the curves). The variable

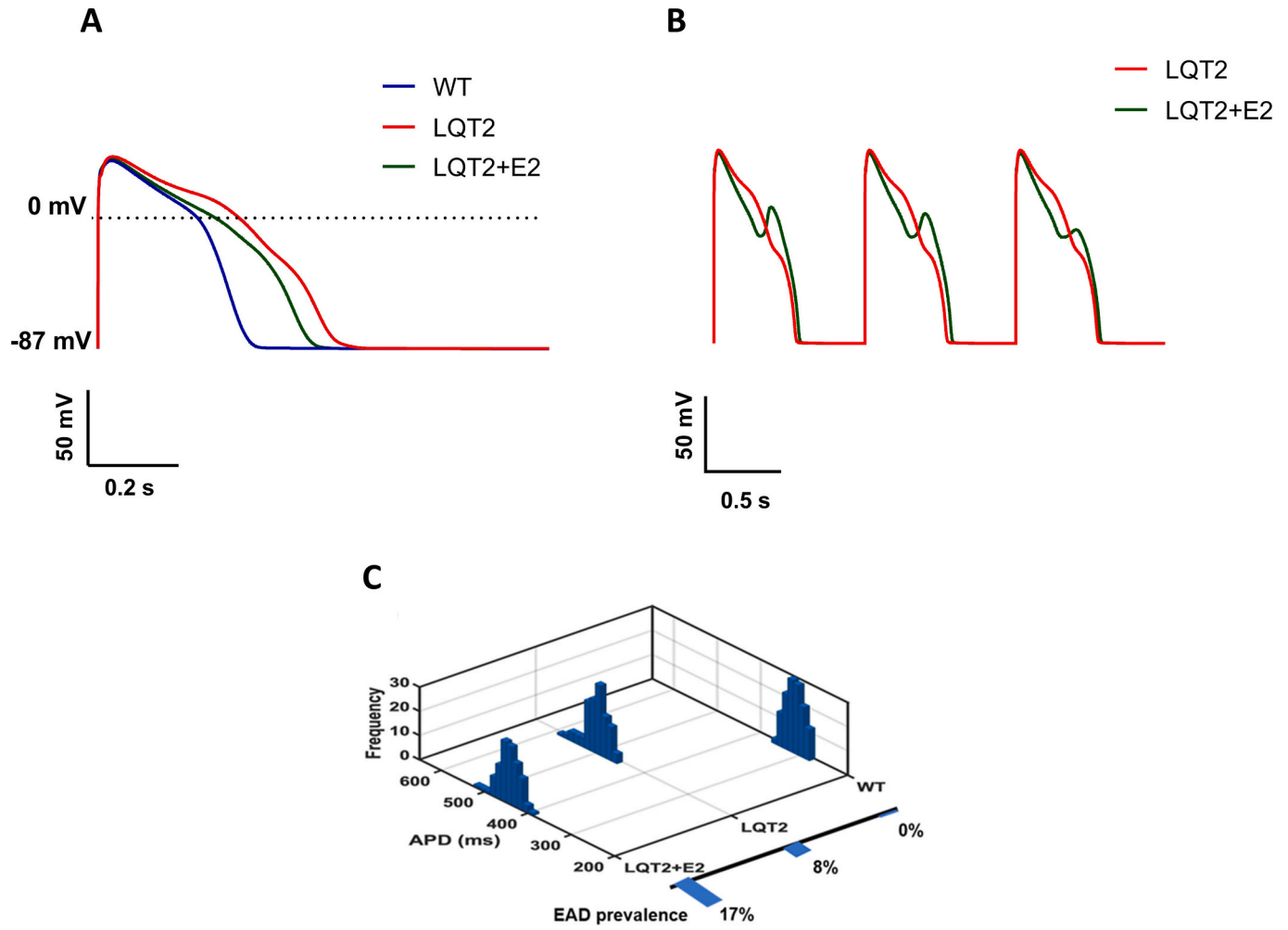

Fig. 6. Modelling results. (A) Mean AP contours (at 1 Hz) for the 3 model populations: wild type (WT, blue trace); LQT2 mutant (I_{Kr} reduction + negative I_{CaL} activation shift + τ_{rec} increase; red trace) and LQT2 + E2 (partial recovery of all I_{CaL} parameters modified by LQT2; green trace). (B) Comparison of LQT2 AP contours before and after E2 (shortened, but with EADs); (C) distributions and EADs prevalence (%) for the three model populations. (For interpretation of the references to colour in this figure legend, the reader is referred to the web version of this article.)

distance between the curves and the colour code (blue no EADs, yellow EADs) denote how steeply EADs prevalence depends on the combination between the two parameters.

4. Discussion

The results of this study have identified a major contribution of changes in I_{CaL} gating to the electrophysiological phenotype of a KCNH2 pore mutation, including APD prolongation and EADs facilitation. E2 opposed all mutation's effect on I_{CaL} gating, thus shortening APD, i.e. an apparently protective effect; nonetheless, EADs prevalence tended to increase with E2, which recapitulates the patient's phenotype. This apparent paradox (EADs persistence despite APD shortening) involved E2 reversal of mutation's effect on the kinetics of I_{CaL} recovery which, in the absence of E2, limited I_{CaL} availability during the AP plateau. Reproduction of experimental findings in a computational human model confirmed this interpretation, highlighting the exquisite sensitivity of EADs to changes in I_{CaL} kinetics. Normality of the expression of channels and E2 receptors in the patient-derived cardiomyocytes point to an entirely functional origin of the mutation's clinical phenotype.

4.1. I_{Kr} differences between LQT2 and WT cells

In WT cells I_{Kr} during the activating step had its typical rectifying profile, its maximal conductance was relatively small, but consistent with that we previously found in hiPS-CMs [3]. In LQT2 cells I_{Kr} was largely unmeasurable, as previously reported for the G628S-KCNH2 mutation [10]. Absence of the current despite unchanged expression of the KCNH2 protein is expected from a pore mutation, affecting the protein conductive properties, rather than its expression.

4.2. I_{CaL} differences between LQT2 and WT cells

The observation of differences in I_{CaL} V-dependent gating between cells carrying a K^+ channel mutation and WT ones was serendipitous, nonetheless, potentially relevant to the phenotype and of mechanistic interest. As an afterthought, a hint to the contribution of something beyond I_{Kr} insufficiency to LQT2 phenotype comes already from the extent of c_APD (and QTc) prolongation. Indeed, the normalized c_APD difference between WT and LQT2 cells in the present study (+142%) exceeds by far that reportedly induced by I_{Kr} blockade in hiPS-CMs (+31%–36%) [16,17].

The unexpectedly large APD (and QT) prolongation was associated with a relatively low incidence of EADs. The observation led to detailed investigation of I_{CaL} gating, which disclosed enhancement of the I_{CaL} "window" and slowing of I_{CaL} recovery from inactivation. Population-based model simulations confirmed these formers as an adequate cause of excess APD prolongation and revealed an exquisite sensitivity of

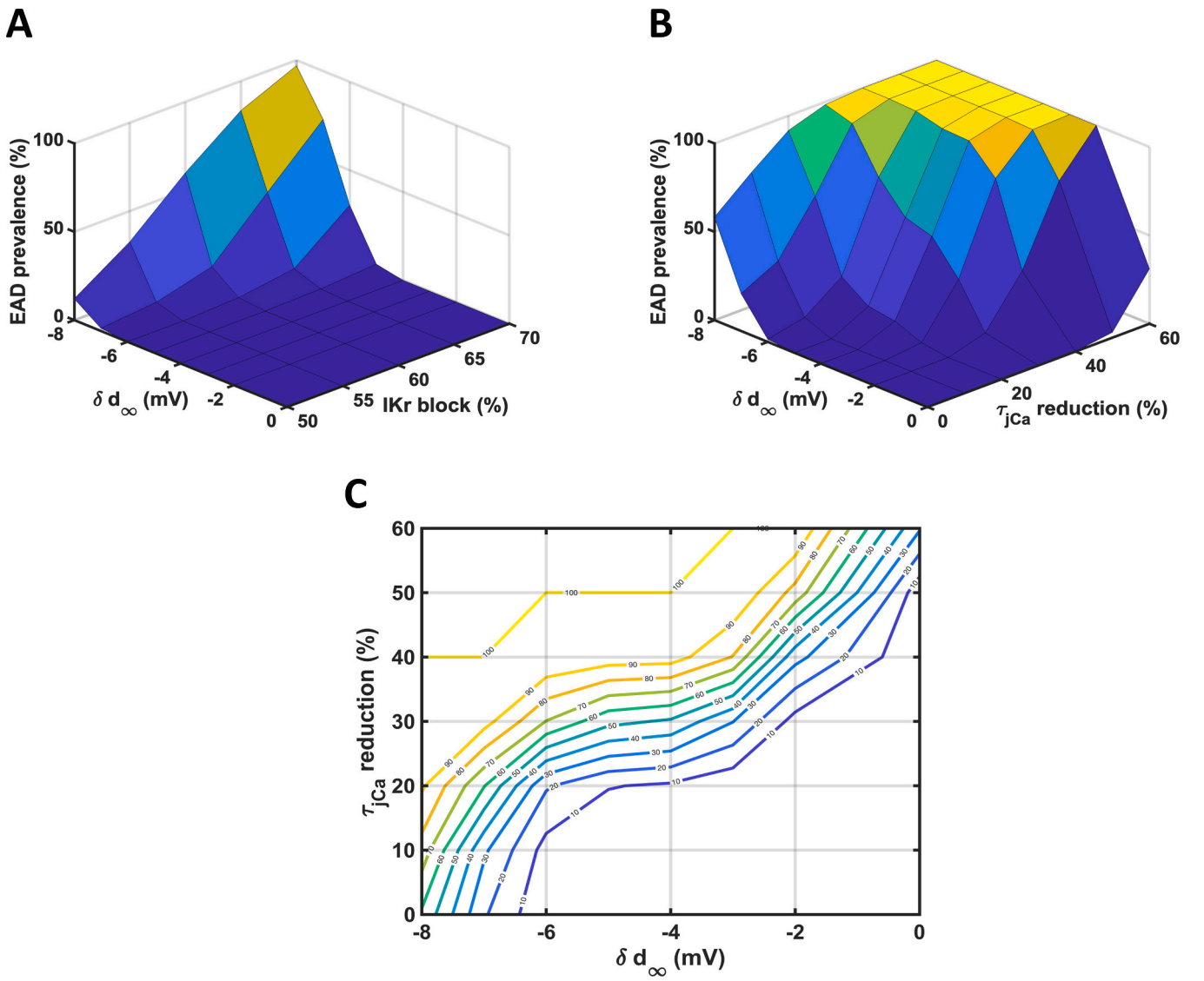

Fig. 7. Sensitivity analysis for the effect of model parameters on EADs prevalence. (A) EADs prevalence as a function of changes in I_{Kr} conductance and shift in the I_{CaL} steady-state activation curve (δd_∞, τ_{rec} set at its WT value). (B) EADs prevalence as a function of changes in I_{CaL} recovery time constant (τ_{rec}) and shift in the steady-state activation curve (δd_∞; I_{Kr} block set at 60%). (C) Isolines of EADs prevalence corresponding to the surface plot shown in Panel B.

EADs incidence to I_{CaL} recovery kinetics in the context of deficient I_{Kr}.

Whatever their mechanism, the detected changes in I_{CaL} gating may substantially contribute to the phenotype of LQT2 cells, both in terms of repolarization delay and arrhythmia facilitation.

4.3. E2 effects

Based on current knowledge of estrogen modulation of ion channels, E2 effects on repolarization of mutant hiPS-CMs were unexpected: 1) E2 shortened c_APD instead of prolonging it; 2) c_APD shortening was not associated with the expected decrease in EADs prevalence, a clear trend to increase was observed instead; 3) c_APD shortening was not caused to changes in channel expression after E2 stimulation. Notably, E2 affected neither c_APD, nor I_{CaL} parametrs in WT hiPS-CMs, thus implying a mutation-specific action.

Detailed evaluation of E2 effects on I_{CaL} allowed to reconcile these apparent discrepancies by disclosing changes in channel gating, which account for both APD shortening and EADs facilitation. This leads to the general conclusion that EADs facilitation is compatible with APD shortening, provided that I_{CaL} V-dependent kinetics is suitably modulated. This is in full agreement with the "non-equilibrium gating" mode of EADs generation [14,18].

The I_{CaL} gating abnormalities associated with the KCNH2 mutation were rather complex, including a shift in steady state V-dependency and changes in the recovery kinetics. The observation that these changes coexisted, and were simultaneously reversed by E2, suggests a shared mechanism targeted by the hormone.

Studies in animal models report estrogen modulation of multiple currents involved in cardiac repolarization and arrhythmogenesis, including I_{Kr}, and I_{CaL}, by both genomic and non-genomic modulation [5]. Albeit with exceptions [19], the overall direction of modulation is mostly compatible with APD prolongation and EADs facilitation (e.g. I_{Kr} downregulation and I_{CaL} upregulation), which was proarrhythmic in the context of LQT2 [20]. In the present study, E2 neither prolonged repolarization in WT cells nor changed I_{Kr} and I_{CaL} densities; whether differences in cell type (maturity), hormone concentration or exposure mode may account for the difference is unclear. E2 may also upregulate I_{Ks} [20], not measured in the present study, which might theoretically contribute to the observed APD shortening. However, I_{Ks} is reportedly very small in hiPS-CMs [3] and E2 effects on I_{net} are more suggestive of I_{CaL} modulation, which numerical simulations proved to be necessary and quantitatively adequate.

Cellular estrogen effects can be genomic or non-genomic (post-transcriptional); whereas intracellular receptors are more commonly involved in the former, membrane (G-protein associated) ones prevail in the latter. In the present experiments, E2 effects developed over a relatively short exposure time, which is more compatible with non-genomic modulation. This hypothesis seems to be supported by the observation that the expression of KCNH2 and CACNA1C did not show significant changes under the same conditions used for electrophysiological experiments.

Whereas in isolated cells the observed effects are clearly attributable to E2 challenge, in-vivo estrogen administration may perturb endocrine signalling in a more complex fashion. This may include feed-back suppression of basal androgen secretion, which is pronounced in the polycystic ovary syndrome and known to modulate repolarization with antiarrhythmic effects [5]. Therefore, arrhythmia facilitation in the index patient might depend on combined estrogen challenge and androgens withdrawal. At any rate, the results point to a causative effect of estrogen administration in arrhythmia induction, a conclusion of therapeutic significance in this case.

4.4. Experimental vs computational results

Model simulations confirmed the primary role of changes in I_{CaL} in accounting for APD prolongation in LQT2 cells. They also reproduced the unexpected observation of simultaneous APD shortening and EADs facilitation by E2 and attributed it to restoration of fast I_{CaL} recovery on the background of a still slowed repolarization. Such results are essential in translating observations obtained in hiPS-CM to the context of mature electrophysiology.

When applied to the model with the observed magnitude, mutation-induced changes in gating parameters resulted in excessive modification of APD contour and EADs prevalence. A quantitative discrepancy was expectable considering that experimental results obtained in hiPS-CM were applied to a model of mature human cardiomyocyte. Therefore, the magnitude of changes in I_{CaL} parameters implemented in the model was adjusted to approach the observed changes in APD and EADs prevalence. On the other hand, it is impossible to say whether the model or the hiPS-CMs response better approximates, in quantitative terms, that of mature human cardiomyocytes.

Numerical simulations disclose that, along with changes in I_{Kr} conductance, shifts of the I_{CaL} activation curve (δd_∞) and changes in I_{CaL} recovery kinetics (τ_{rec}) have a strong impact on EADs prevalence (Fig. 7). Notably, δd_∞ had a remarkably smaller impact on APD_{90} (Fig. S11) thus stressing that APD prolongation and EADs are not necessarily associated. This recapitulates the unexpected experimental observation that, albeit shortening APD_{90}, E2 failed to reduce the prevalence of EADs (Fig. 2).

We previously reported that APD prolongation per se may facilitate Ca^{2+} overload [21], thus opening the possibility that in the present context EADs might reflect spontaneous Ca^{2+} release events [22]. Albeit the model does incorporate intracellular Ca^{2+} handling, the interpretation of EADs limitation/facilitation entirely relies on electrical abnormalities (repolarization delay and I_{CaL} gating). Therefore, although the present findings do not rule out the possibility of EADs triggering by spontaneous Ca^{2+}release events, they do not provide evidence to it.

5. Translational relevance

The results obtained lead to several conclusions of practical relevance. 1) Even in the absence of genetic CACNA1C abnormalities, changes in I_{CaL} gating may substantially contribute to LQT2 phenotype. 2) I_{CaL} changes were almost entirely reversed by E2, which might suggest a protective effect of estrogen stimulation; however, “normalization” of recovery kinetics by the hormone in the context of the LQT2 phenotype, was associated with EADs persistence. 3) APD shortening does not necessarily protect from EADs. Our results do not prove causality between estrogen therapy and arrhythmia spells; they just indicate that causality is plausible and disclose a mechanism for it.

6. Study limitations

Since the working hypothesis focused on E2 effects, rather than on LQT2 vs WT differences, the study design did not include an isogenic WT control; indeed, the hypothesis of an I_{CaL} perturbations in LQT2 cells was prompted, *in itinere*, by the incoming results. Thus, the study design is inadequate to prove that the KCNH2 mutation alone accounted for the LQT2 vs WT phenotypic differences. On the other hand, the results were reproduced across several cell differentiation batches, neither genotype included abnormalities in CACNA1C genes, I_{CaL} density was almost identical between them (Fig. 3), and the differences concerned entirely gating (functional) properties. Moreover, such differences could be reversed in LQT2 cells by E2, which reinstated properties close to those of WT cells (Figs. 3 and 4). All this, makes unlikely that factors other than the KCNH2 mutation may account for the divergence of I_{CaL} properties between WT and LQT2 cells.

hiPS-CMs may exhibit immature structure and electrophysiological properties; nonetheless, they afford the best chance to study disease mechanisms in the context of patients' genotype. To translate the observations made in hiPS-CMs to mature electrical activity was the purpose of numerical simulations, for which a model of human adult ventricular myocyte was chosen. Particularly for what concern EADs prevalence, response to I_{Kr} and I_{CaL} changes was sharper in the model than in hiPS-CMs, thus the changes observed in hiPS-CMs had to be scaled down to preserve model stability. Possibly because of hiPS-CMs immaturity, 10 nM E2, at the upper extreme of the physiological range, is required to affect repolarization in these cells [6] and was therefore adopted in the present study.

Slightly subphysiological temperature was required to achieve optimal preparation stability and minimize current run-down. Lower temperature may slow current kinetics and prolong APD; nonetheless, the AP parameters measured from WT myocytes are in line with physiological ones and c_APD of LQT2 cells is close to patient's QTc. Since the temperature was kept constant in all comparisons, its value cannot account for the observed differences.

Authors' contribution

This work results from the collaboration between groups expert in cellular electrophysiology (led by **A. Zaza**) and cell biology (led by **M. Gnecchi**) respectively.

CRediT authorship contribution statement

C. Maniezzi: Writing – review & editing, Visualization, Methodology, Investigation, Formal analysis, Data curation. **F. Bastaroli:** Investigation, Formal analysis. **I. Anzaldi:** Investigation, Formal analysis. **C. Florindi:** Investigation, Formal analysis. **V. Dusi:** Conceptualization. **A. Dosio:** Investigation, Formal analysis. **M. Mura:** Visualization, Investigation, Formal analysis, Data curation. **J. Tomek:** Software, Methodology, Conceptualization. **J.F. Rodriguez Matas:** Writing – review & editing, Visualization, Software, Methodology, Investigation. **F. Lodola:** Writing – review & editing, Supervision, Methodology. **M. Gnecchi:** Writing – review & editing, Supervision, Methodology, Funding acquisition. **A. Zaza:** Writing – original draft, Supervision, Project administration, Methodology, Funding acquisition, Conceptualization.

Declaration of generative AI and AI-assisted technologies in the writing process

The authors did not use generative AI or AI-assisted technologies in the development of this manuscript.

Declaration of competing interest

None.

Acknowledgement

This work was funded by Fondo di Ateneo per la Ricerca (2024-ATEQC-0032) from University of Milano-Bicocca and the Italian Ministry of Health "PRIN 2022" project number 2022-NAZ-0249-PNRR to A. Zaza. hiPS generation, hiPS differentiation into CMs, hiPS-CMs preparation and molecular studies were funded by Leducq Foundation for Cardiovascular Research [18CVD05] 'Towards Precision Medicine with Human iPSs for Cardiac Channelopathies', and by the Italian Ministry of Health, "Ricerca Corrente" project number 08064017 to M. Gnecchi.

Appendix A. Supplementary data

Supplementary data to this article can be found online at https://doi.org/10.1016/j.yjmcc.2026.07.004.

References

[1] J.R. Giudicessi, M.J. Ackerman, Determinants of incomplete penetrance and variable expressivity in heritable cardiac arrhythmia syndromes, Transl. Res. 161 (1) (2013) 1–14.
[2] C. Ronchi, J. Bernardi, M. Mura, M. Stefanello, B. Badone, M. Rocchetti, et al., NOS1AP polymorphisms reduce NOS1 activity and interact with prolonged repolarization in arrhythmogenesis, Cardiovasc. Res. 117 (2020) 472–483.
[3] Y.K. Lee, L. Sala, M. Mura, M. Rocchetti, M. Pedrazzini, X. Ran, et al., MTMR4 SNVs modulate ion channel degradation and clinical severity in congenital long QT syndrome: insights in the mechanism of action of protective modifier genes, Cardiovasc. Res. 117 (2020) 767–779.
[4] A.J. Sauer, A.J. Moss, S. McNitt, D.R. Peterson, W. Zareba, J.L. Robinson, et al., Long QT syndrome in adults, J. Am. Coll. Cardiol. 49 (3) (2007) 329–337.
[5] K.E. Odening, G. Koren, How do sex hormones modify arrhythmogenesis in long QT syndrome? Sex hormone effects on arrhythmogenic substrate and triggered activity, Heart Rhythm. 11 (11) (2014) 2107–2115.
[6] J. Huo, F. Wei, C. Cai, B. Lyn-Cook, L. Pang, Sex-related differences in drug-induced QT prolongation and Torsades de pointes: a new model system with human iPSC-CMs, Toxicol. Sci. 167 (2) (2019) 360–374.
[7] T. O'Hara, L. Virag, A. Varro, Y. Rudy, Simulation of the undiseased human cardiac ventricular action potential: model formulation and experimental validation, PLoS Comput. Biol. 7 (5) (2011) e1002061.
[8] J. Elliott, M.K. Belen, L. Mainardi, J.F. Rodriguez Matas, A comparison of regional classification strategies implemented for the population based approach to modelling atrial fibrillation, Mathematics 9 (14) (2021).
[9] A. Muszkiewicz, O.J. Britton, P. Gemmell, E. Passini, C. Sanchez, X. Zhou, et al., Variability in cardiac electrophysiology: using experimentally-calibrated populations of models to move beyond the single virtual physiological human paradigm, Prog. Biophys. Mol. Biol. 120 (1–3) (2016) 115–127.
[10] M. Brunner, X. Peng, G.X. Liu, X.Q. Ren, O. Ziv, B.R. Choi, et al., Mechanisms of cardiac arrhythmias and sudden death in transgenic rabbits with long QT syndrome, J. Clin. Invest. 118 (6) (2008) 2246–2259.
[11] M.D. Drici, T.R. Burklow, V. Haridasse, R.I. Glazer, R.L. Woosley, Sex hormones prolong the QT interval and downregulate potassium channel expression in the rabbit heart, Circulation 94 (6) (1996) 1471–1474.
[12] J. Kurokawa, M. Tamagawa, N. Harada, S. Honda, C.X. Bai, H. Nakaya, et al., Acute effects of oestrogen on the guinea pig and human IKr channels and drug-induced prolongation of cardiac repolarization, J. Physiol. 586 (12) (2008) 2961–2973.
[13] S. Mahmoodzadeh, E. Dworatzek, The role of 17beta-Estradiol and Estrogen receptors in regulation of Ca(2+) channels and mitochondrial function in cardiomyocytes, Front. Endocrinol. (Lausanne) 10 (2019) 310.
[14] C.T. January, J.M. Riddle, Early afterdepolarizations: mechanism of induction and block. A role for L-type Ca^{2+} current, Circ. Res. 64 (1989) 977–990.
[15] M. Rocchetti, L. Sala, L. Dreizehnter, L. Crotti, D. Sinnecker, M. Mura, et al., Elucidating arrhythmogenic mechanisms of long-QT syndrome CALM1-F142L mutation in patient-specific induced pluripotent stem cell-derived cardiomyocytes, Cardiovasc. Res. 113 (5) (2017) 531–541.
[16] M.X. Doss, J.M. Di Diego, R.J. Goodrow, Y. Wu, J.M. Cordeiro, V.V. Nesterenko, et al., Maximum diastolic potential of human induced pluripotent stem cell-derived cardiomyocytes depends critically on I(Kr), PLoS One 7 (7) (2012) e40288.
[17] L. Zwi, O. Caspi, G. Arbel, I. Huber, A. Gepstein, I.H. Park, et al., Cardiomyocyte differentiation of human induced pluripotent stem cells, Circulation 120 (15) (2009) 1513–1523.
[18] C.E. Clancy, M. Tateyama, H. Liu, X.H. Wehrens, R.S. Kass, Non-equilibrium gating in cardiac Na+ channels: an original mechanism of arrhythmia, Circulation 107 (17) (2003) 2233–2237.
[19] L. Anneken, S. Baumann, P. Vigneault, P. Biliczki, C. Friedrich, L. Xiao, et al., Estradiol regulates human QT-interval: acceleration of cardiac repolarization by enhanced KCNH2 membrane trafficking, Eur. Heart J. 37 (7) (2016) 640–650.
[20] K.E. Odening, B.R. Choi, G.X. Liu, K. Hartmann, O. Ziv, L. Chaves, et al., Estradiol promotes sudden cardiac death in transgenic long QT type 2 rabbits while progesterone is protective, Heart Rhythm. 9 (5) (2012) 823–832.
[21] C. Ronchi, B. Badone, J. Bernardi, A. Zaza, Action potential prolongation, beta-adrenergic stimulation, and angiotensin II as Co-factors in sarcoplasmic reticulum instability, Front. Physiol. 9 (2018) 1893.
[22] Z. Zhao, H. Wen, N. Fefelova, C. Allen, A. Baba, T. Matsuda, et al., Revisiting the ionic mechanisms of early afterdepolarizations in cardiomyocytes: predominant by Ca waves or Ca currents? Am. J. Physiol. Heart Circ. Physiol. 302 (8) (2012) H1636–H1644.